Earth, Planets and Space

FULL PAPER Open Access

Estimation of source parameters using a non-Gaussian probability density function in a Bayesian framework

Nana Yoshimitsu[1*], Takuto Maeda[2] and Tomonari Sei[3]

Abstract

Source parameters represent key factors in seismic hazard assessment and understanding source physics of earthquakes. In addition to conventional grid search approach to estimate source parameters, other approaches have been used recently. This study uses a Bayesian framework, the Markov Chain Monte Carlo method, to estimate source parameters including uncertainty assessment with inter-parameter correlations. The Bayesian calculation method requires to select a probability density function for estimating likelihood and the function can influence calculation reliability. While most studies use a normal distribution, we select an *F*-distribution due to its suitability for the data in ratio form. Using synthetic data and real observations from induced earthquakes in Oklahoma, we compare the calculation steps for spectral fitting and source parameter estimation using the two probability density functions. The sampling distribution and estimated parameters support the assumption that the *F*-distribution is well-suited for spectral ratio analysis. Results further show that a sampling distribution can effectively reveal trade-offs and uncertainty among parameters. Sampling distribution trends also reveal data quality criteria that can be used to refine results.

Keywords MCMC, Stress drop, Source parameter

*Correspondence:
Nana Yoshimitsu
yoshimitsu.nana.6i@kyoto-u.ac.jp
Full list of author information is available at the end of the article

Graphical Abstract

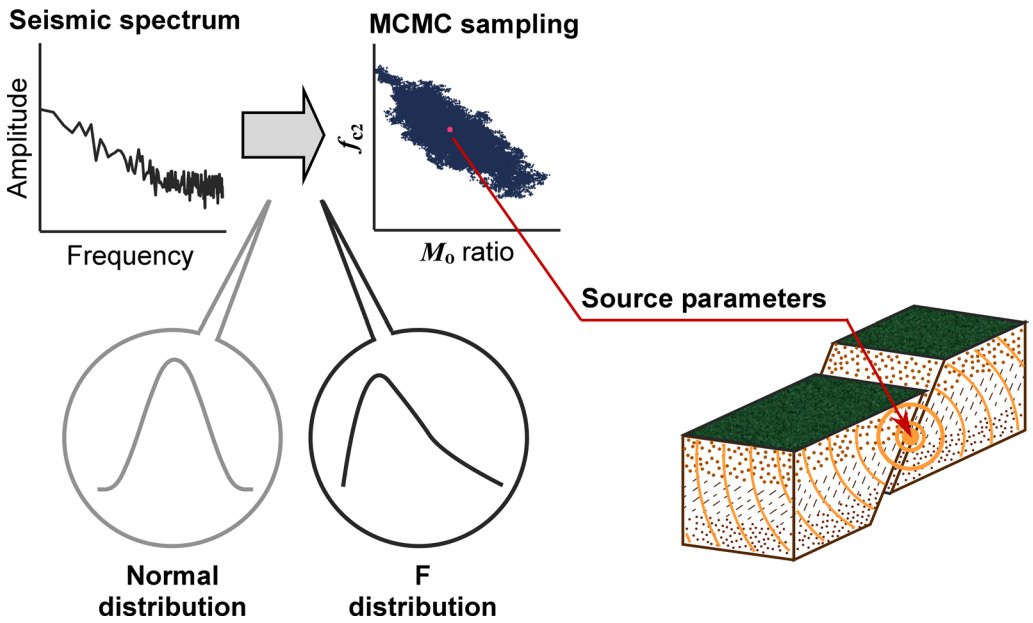

Main text

Introduction

As a critical factor in seismology, earthquake stress drops have been estimated in various areas in the world. In seismic hazard assessment, the stress drop of an earthquake can constrain ground motion predictions for future earthquakes (e.g., Cotton, et al. 2013; Baltay et al. 2019). Estimation of future earthquake shaking requires the stress drop value in the target region that is investigated from the past earthquakes. Because stress drop depends on seismic source characteristics, it is also important for deepening our understanding of how earthquakes are generated (e.g., Goebel et al. 2015; Chu et al. 2019; Yoon et al. 2019). Some studies have suggested the possibility of a depth dependency in stress drop (e.g., Oth 2013), while other studies have searched for other mechanisms or dependencies (e.g., Allmann and Shearer 2009) by analyzing many small earthquakes within a target region. Some studies have proposed that the depth dependency of the stress drop is an artifact of calculation (e.g., Abercrombie et al. 2021). If stress drops of small earthquakes estimated in a target region show a significant relationship with parameters that reflect crustal conditions, this could advance understanding of the relationship between crustal characteristics and seismic behavior. Estimation uncertainty, however, can obscure characteristics in source parameters. Stress drop estimates in the target region sometimes fluctuate three or more orders (e.g., Hanks 1977). Numerous studies have sought the better estimation and utilization of stress drop.

Stress drop, seismic moment, and corner frequency are called source parameters since they are primarily derived from characteristics of the seismic source. Stress drop is obtained from estimates of seismic moment and corner frequency (Eshelby 1957). Seismic moment and corner frequency are obtained through comparison with a source spectrum that derives from the theoretical model and the observed data (Abercrombie 1995). The observed spectra bear the influence of seismic wave propagation through the earth medium and amplification within near-surface sediments. Estimation methods typically use a spectral ratio of two co-located earthquakes to cancel out the path and instrumental effects (Hough 1997). Recent studies have proposed the use of coda waves in source parameter analysis. Coda waves represent the later part of the seismic waveforms that are generated by scattering of the direct waves and interpreted as having lost information of the source radiation pattern and directivity (Mayeda et al. 2007). These analyses are conventionally performed by grid-search methods.

Bayesian statistics are increasingly used in various types of data analysis as the different approach from the conventional method. Bayesian approaches evaluate the estimation quality through probabilistic analysis of parameters relative to expectations. Monte Carlo

methods have been used in geophysics since the 1960s (Sambridge and Mosegaard 2002). Markov Chain Monte Carlo methods (MCMC) use an algorithm that samples probability distributions using Markov chains to generate a high-dimensional random sampling in a Bayesian framework (Metropolis et al. 1953). A Markov Chain is a stochastic process that describes a sequence of possible events whose probability depends only on the state of the previous event. Geophysicists have begun to use MCMC in seismological analysis (e.g., Lomax et al. 2000; Roy and Romanowicz 2017; Berg et al. 2020), and several previous studies have demonstrated successful use of MCMC in estimating seismic source parameters including stress drop. A recent study by Godano et al. (2015) used MCMC to estimate source parameters for seismic activity in western areas of the Corinth Rift. Another study, Wu and Chapman (2017) also used this method to estimate the stress drop of earthquakes in Mineral, Virginia.

Conventional grid-search techniques sequentially evaluate all combinations of possible source parameter values to find the best value for explaining the model (e.g., Yamada et al. 2007; Kwiatek et al. 2011). In spite of its simplicity and easy implementation, this method may sample regions far the best estimation points. Inversions in high-dimensional spaces necessary for producing satisfactory solutions may become computationally infeasible when using a coarse grid. The MCMC approach uses a selective search that prioritizes higher probability results so as to search only the regions around the high probability points. This reduces computational overhead and realizes calculation efficiencies in high-dimensional spaces. The process can exclude cases where the target posterior distribution is multimodal thereby causing the MCMC to converge around a local probability maximum. Because MCMC methods sample a stationary distribution, they allow for evaluation of trade-offs among source parameters and other results including uncertainty terms.

As a Bayesian algorithm, MCMC provides probabilistic estimates of parameters and their uncertainties. Calculation of MCMC requires an initial input probability density function which can influence results. Accurate uncertainty estimates require selection of an appropriate probability density function. Previous studies using MCMC method selected a normal distribution to estimate seismic source parameters and stress drops (e.g., Wu and Chapman 2017). While the normal distribution is the most popular probability density function, phenomena under investigation may not follow a normal distribution. The present study, we use a novel probability density function in the source parameter estimation that is theoretically more appropriate than the conventional normal distribution. The next section describes the concept of the probability density function choice, and we compare results with those generated by a normal distribution and a proposed distribution.

Stress drop estimation with MCMC calculation

Source parameters of seismic moment (M_0) and corner frequency (f_c) are calculated from the displacement spectrum of seismic records. The term M_0 indicates the size of the seismic event which relates to the spectral amplitude of the low-frequency asymptote. The corner frequency, f_c, is inversely proportional to the fault dimension. Stress drop ($\Delta\sigma$) is estimated from M_0 and f_c using the following equation (after Eshelby 1957):

$$\Delta\sigma \sim \frac{7}{16} M_0 f_c^3. \tag{1}$$

A seismic waveform is represented by a convolution of source, path, and instrumental effects. Recent studies on stress drops use spectral ratios of co-located earthquakes to cancel out the path and instrumental effects (e.g., Imanishi and Ellsworth 2006; Huang et al. 2017). The far-field S-wave amplitude spectrum (U) of an earthquake is expressed as follows (Aki and Richards 1980):

$$U(f) = \frac{\Omega_0 e^{-(\pi f t/Q)}}{\left[1 + (f/f_c)^{\gamma n}\right]^{1/\gamma}}, \tag{2}$$

where $\Omega_0$is the amplitude of the low-frequency asymptote, f is frequency, f_c is the corner frequency of the S wave spectrum, t is the propagation time, Q is the quality factor, n is the high-frequency fall-off rate, and γ is a constant that controls the sharpness of the spectra corner. Previous studies have proposed several types of seismic source models and here we use the most commonly adopted Brune model (Brune 1970, 1971). This model assumes a circular crack of the finite dimensions, and the spectral shape estimated from this model describes the shape of the observed spectra in wide region of the world. The Brune model assumes $n = 2$, $\gamma = 1$ in Eq. (2), and the proportional constant $k = 0.37$ between the crack radius and S-wave velocity divided by f_c. Then, the spectral ratio for a pair of earthquakes is described as follows:

$$\frac{U_1(f)}{U_2(f)} = \frac{\Omega_{01} e^{-(\pi f t/Q)}}{\Omega_{02} e^{-(\pi f t/Q)}} \frac{\left[1 + (f/f_{c2})^2\right]}{\left[1 + (f/f_{c1})^2\right]}. \tag{3}$$

Subscripts of 1 and 2 in the equation, respectively, indicate the larger and smaller earthquake. Using the proportional relationship between Ω_0 and M_0, Eq. (3) can be simplified to:

$$\frac{U_1(f)}{U_2(f)} = \frac{M_{01}}{M_{02}} \frac{\left[1 + \left(f/f_{c2}\right)^2\right]}{\left[1 + \left(f/f_{c1}\right)^2\right]}. \tag{4}$$

To calculate a stress drop, the seismic moments (M_{01}andM_{02}), the corner frequency of a large earthquake (f_{c1}), and the corner frequency of a small earthquake (f_{c2}) in Eq. (4) need to be estimated. As we described in the introduction, MCMC methods depend on selection of probability density function used as input. Here, we propose the use of an *F*-distribution due to its suitability in dealing with ratios of the two data series expressed in Eq. (4). In general, the power spectrum of a seismic waveform ($P = U^2$) is represented by the real part (a) and imaginary part (b) of the Fourier spectrum:

$$P_{data}(f) = \frac{1}{T}\left(a(f)^2 + b(f)^2\right). \tag{5}$$

In this expression, P_{data} represents the observed power spectrum and T indicates the time window of the signal. We suppose that the real part of the spectrum $a(f)$ and the imaginary part of the spectrum $b(f)$ are independent of each other and follow a Gaussian distribution. At this point, we set the model-predicted power spectrum (P_{model}) that is the square of the amplitude spectrum $U(f)$ in Eq. (4) and not a random variable. Here, we assume $a = \sigma_d \times A$, $b = \sigma_d \times B$ where A and B follow a standard normal distribution. Then, $P_{data}(f) = \frac{\sigma_d}{T}\left(A(f)^2 + B(f)^2\right)$. If the variance σ_d adheres to the relationship $\sigma_d = T \bullet P_{model}(f)$, $P_{data}(f)/P_{model}(f)$ approximates a Chi-distribution. The Chi-square distribution represents the sum of squared standard Gaussian variables, where the number of Gaussian variables is referred to as degrees of freedom. Then, the ratio between observed (P_{data}) and the model-predicted power spectrum (P_{model}) obeys the Chi-square (χ^2) distribution:

$$\chi^2 = \frac{P_{data}(f)}{P_{model}(f)}. \tag{6}$$

The ratio between two independent Chi-square random variables which indicate different events is called an *F*-distribution (e.g., Casella and Berger 2002):

$$F(k_1, k_2) = \frac{\chi_1^2(k_1)/k_1}{\chi_2^2(k_2)/k_2}. \tag{7}$$

Both degrees of freedom k_1 and k_2 are equal to two, in keeping with the real and imaginary parts of a seismic wave. Equation (7) is simplified to the ratio of two different events such that the denominator and numerator are expressed by the power spectral ratio between model prediction and observed data by Eq. (6):

$$\begin{aligned} F(2,2) &= \frac{\chi_1^2(2)/2}{\chi_2^2(2)/2} \\ &= \frac{P_{1data}/P_{1model}}{P_{2data}/P_{2model}} \\ &= \frac{P_{1data}/P_{2data}}{P_{1model}/P_{2model}}. \end{aligned} \tag{8}$$

Here, P_{imodel} represents power spectrum whose ratio is explicitly written using Eq. (4) as follows:

$$\begin{aligned} E\left(f; \frac{M_{01}}{M_{02}}, f_{c1}, f_{c2}\right) &\equiv \frac{U_1(f)}{U_2(f)} \\ &= \sqrt{\frac{P_{1model}}{P_{2model}}} \\ &= \left(\frac{M_{01}}{M_{02}}\right)\frac{1 + \left(f/f_{c2}\right)^2}{1 + \left(f/f_{c1}\right)^2}. \end{aligned} \tag{9}$$

Thus, the ratio between observed power spectrum ratio P_{1data}/P_{2data} and E^2 obeys the $F(2,2)$ distribution. Equation (8) resembles spectral ratios typically used for source parameter estimation and takes the form of an *F*-distribution. This study further compared results generated by both *F*-distributions and normal distributions used as probability density function.

In every sampling iteration, we calculate likelihood using probability density functions by substituting sample parameters for the ratio of the squared observed amplitude spectrum and the squared theoretical amplitude spectrum. To obtain one likelihood for records from all stations, we use the product of likelihood from each station. The general expression of the probability density function for an *F*-distribution using gamma function Γ is as follows:

$$q(x; k_1, k_2) = \frac{\Gamma\left(\frac{k_1+k_2}{2}\right) x^{\frac{k_1-2}{2}}}{\Gamma\left(\frac{k_1}{2}\right)\Gamma\left(\frac{k_2}{2}\right)\left(1 + \frac{k_1}{k_2}x\right)^{\frac{k_1+k_2}{2}}}\left(\frac{k_1}{k_2}\right)^{\frac{k_1}{2}}, \tag{10}$$

where x is calculated as the power spectral ratio of the observed spectrum divided by the theoretical spectrum. After substituting the degrees of freedom, Eq. (10) simplifies to:

$$q(x; k_1 = 2, k_2 = 2) = \frac{1}{(1+x)^2}, x > 0. \tag{11}$$

This likelihood function makes sense when it has a mode at $x = 0$ because the model parameter also appears in the

Jacobian factor. The likelihood function is then represented with the probability density function as follows:

$$L(M_R, f_{c1}, f_{c2}) = \prod_{j=J_1}^{J_2} \prod_{s=1}^{S} \left\{ q\left(\frac{O_s^2(f_j)}{E^2(f_j; M_R, f_{c1}, f_{c2})} \right) \frac{1}{E^2(f_j; M_R, f_{c1}, f_{c2})} \right\}$$
$$= \prod_{j=J_1}^{J_2} \prod_{s=1}^{S} \left\{ \frac{E^{-2}(f_j; M_R, f_{c1}, f_{c2})}{\left[1 + \left\{ O_s(f_j)/E(f_j; M_R, f_{c1}, f_{c2}) \right\}^2 \right]^2} \right\}. \quad (12)$$

In these expressions, $O_s \sim \sqrt{P_{1data}/P_{2data}}$ represents the amplitude spectral ratio between two earthquakes observed at the s-th station, $M_R \equiv M_{01}/M_{02}$ is the moment ratio, and f_j is discretized frequency. The factor $1/E^2(f_j)$ in Eq. (12) is the Jacobian derived from variable transformation $x = O_s^2(f_j)/E^2(f_j)$ on the probability density function. The probability density function is $q_y(y) = q_x(x)|\frac{dx}{dy}|$, where y denotes $O_s^2(f_j)$. The Jacobian is required to unify the integrals with respect to O_s^2 of the likelihood function.

For comparison, we also perform the analysis assuming a normal distribution. In this case, the probability density function is expressed as:

$$q(x) = \frac{1}{\sqrt{2\pi}\sigma} \exp\left\{ -\frac{(x-\mu)^2}{2\sigma^2} \right\}, \quad (13)$$

where μ is the mean and σ is the standard deviation. The term x in Eq. (13) indicates the logarithm of the amplitude spectral ratio calculated as the observed spectrum divided by the theoretical spectrum. While conventional studies that often use a smoothed amplitude spectrum, this analysis does not use smoothed or stacked spectra in order to avoid violating distribution assumptions.

We use the Metropolis algorithm as a MCMC algorithm (Metropolis et al. 1953), which updates the likelihood function (Eq. (12)) in each iteration. The algorithm requires a proposal density that indicating the probability density function of the transition probability from the current condition to the new status. The proposal density is expressed as $Q(\theta^*|\theta) = Q(\theta|\theta^*)$, where θ and θ^* are the current value and candidate values, respectively. We use the normal random variable $\theta^* = \theta + N(0, \sigma^2)$ as the candidate value. Standard deviations (σ) is used to control the transition rate in the MCMC algorithm. We set the standard deviation to 0.5 for the moment ratio, 0.01 for f_{c1}, and 0.01 for f_{c2}.

Calculations are performed under the assumption of a uniform prior distribution. The prior distribution ranges from 0 to 100 for the moment ratio, from 0 to 15 for f_{c1}, and from 0 to 30 for f_{c2}. The initial inputs for the MCMC algorithm are 70.0 for M_{01}/M_{02}, 1.0 for f_{c1}, and 7.0 for f_{c2}. The candidate value is accepted with probability $\min(1, L_{new}/L)$, where L and L_{new} are the likelihood function evaluated at the current and candidate values, respectively. Each iteration generates a random number $r (0 < r < 1)$ from the uniform distribution:

$$r < \frac{L_{new}}{L}. \quad (14)$$

If Eq. (14) is valid, we renew the source parameters, moment ratio, f_{c1}, and f_{c2}. Otherwise, the previous value remains. This procedure runs for 200,000 iterations using the latter half of 100,000 results for analysis. After all iterations, parameters giving the highest likelihood values are adopted as the best values. After we obtained the moment ratio, we calculate the seismic moment of a small event, M_{02}. We trust the moment magnitude (M_w) of a larger earthquake provided on the website of Saint Louis University Earthquake Center. We could then convert the moment magnitude to M_{01} according to the relationship $M_{01} = 10^{1.5M_{w1}+9.1}$. We then estimate M_{02} by using the estimated moment ratio and M_{01}.

Before applying the method to observational data, we perform MCMC analysis on synthetic data. We assume a large $M_{w1} = 4.0$ earthquake and a smaller $M_{w2} = 3.0$ earthquake to give a moment ratio of 31.6 in generating synthetic spectral ratios. We set f_{c1} =1.3 Hz from the previous study (Yoshimitsu et al. 2019) for the corner frequency of the large event and $f_{c2} = 4.1$ Hz for the corner frequency of the smaller event. These parameters give a stress drop of about 0.66 MPa. We then calculate a base spectral ratio by using these values. We assume Green's function of all stations cancel out perfectly by introducing base spectral ratio. This assumption helps isolate source effects. To introduce noise, we generate two random number sequences. Two values selected from each noise sequence are used to generate two Chi-square distributions and calculate an F-distribution with two degrees of freedom. This noise is added to the base spectral ratio, and we are treated as a synthetic spectral ratio. One hundred sets of 17 spectral ratios are generated to simulate 100 seismic events recorded by 17 different stations. For the calculation, both an F-distribution and normal distribution are used as the probability density function. The

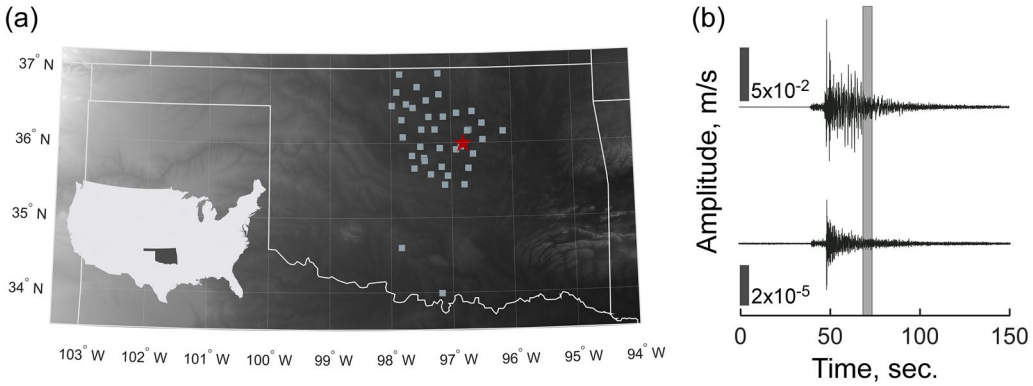

Fig. 1 **a** Center of the event cluster and station locations. The red star indicates the centroid of the cluster. Squares indicate the location of stations used in this study. The bottom left image indicates the contiguous United States (light gray) and the area of the State of Oklahoma (black). **b** Example of a waveform from a large event (top) and a small event (bottom). The top waveform represents the event in Table 1b, and the bottom waveform represents the no.1 event in Table 1a. Both were recorded at station OK025. The rectangle in the middle portion of seismograms indicates the window used in the analysis

Table 1 (a) Event list in a cluster. Rows list year, month, day, hour, minute, second, latitude (degrees), longitude (degrees), depth (km), and magnitude. Event numbers with thin characters indicate an event not selected. (b) Event information of a large earthquake

Event num	Y	M	D	H	M	S	Lat	Lon	Dep	Mag
1	2015	5	29	11	8	41	35.99	− 96.8	3.7	2.7
2	2015	6	13	9	26	14	35.98	− 96.81	3.5	2.3
3	2015	9	16	2	30	2	35.99	− 96.81	3.6	3.7
4	**2015**	**9**	**16**	**6**	**20**	**4**	**35.99**	**− 96.8**	**3.2**	**2.6**
5	**2015**	**9**	**18**	**9**	**33**	**0**	**35.99**	**− 96.8**	**3.5**	**3**
6	**2015**	**9**	**19**	**5**	**16**	**27**	**35.99**	**− 96.8**	**3.6**	**3**
7	**2015**	**9**	**19**	**5**	**20**	**3**	**35.99**	**− 96.8**	**3.9**	**3.1**
8	**2015**	**9**	**19**	**19**	**15**	**26**	**35.99**	**− 96.8**	**3.7**	**2.7**
9	2015	9	25	1	59	4	35.99	− 96.79	4.4	3.1
10	**2015**	**9**	**27**	**21**	**59**	**43**	**35.99**	**− 96.8**	**4.3**	**3.6**
11	**2015**	**9**	**27**	**21**	**59**	**43**	**35.99**	**− 96.8**	**4.2**	**3.2**
12	2015	10	8	2	45	30	35.99	− 96.8	4	3
13	**2015**	**10**	**10**	**23**	**41**	**21**	**35.98**	**− 96.81**	**3.8**	**2.5**
14	**2015**	**10**	**12**	**4**	**1**	**24**	**35.98**	**− 96.81**	**4.4**	**2.9**
15	2015	10	12	8	59	20	35.98	− 96.81	3.9	2.9
16	**2015**	**10**	**31**	**6**	**14**	**5**	**35.99**	**− 96.8**	**3.7**	**3.5**
17	2015	12	11	8	22	41	35.99	− 96.8	3.3	2.7
18	**2015**	**12**	**18**	**2**	**3**	**25**	**35.99**	**− 96.81**	**4**	**3.7**
19	2016	2	4	1	43	18	35.99	− 96.81	3.5	2.5
20	**2016**	**2**	**4**	**2**	**16**	**39**	**35.99**	**− 96.81**	**3.5**	**2.6**

(b)

Y	M	D	H	M	S	Lat	Lon	Dep	Mag
2015	**9**	**18**	**12**	**35**	**17**	**35.99**	**− 96.80**	**3.9**	**4.1**

Rows list year, month, day, hour, minute, second, latitude (degrees), longitude (degrees), depth (km), and magnitude. Event numbers with bold indicate an event not selected

frequency range and the dataset size resemble those of the observed dataset.

Data

We use a cluster of the seismic events referred to 'cluster 0038' occurring in Oklahoma, United States, and reported in Yoshimitsu et al. (2019). Seismic data consisted of broadband velocity records sampled at 100-Hz frequency. The events in the cluster occurred from May 1, 2013, to November 30, 2016, and are recorded by stations operated by the U.S. Geological Survey (USGS), Oklahoma Geological Survey (OGS), and from the Nanometrics Research Network in Oklahoma (Fig. 1a). To cancel out the path, site, and instrumental effects, we use a coda spectral ratio for two events. We select event pairs of a larger event ($M_{w1}=4.1$) and smaller events ($2.3 \leq M_L \leq 3.7$) located within 2 km radius of the large event (Table 1). We use a magnitude difference of greater than 0.4 to differentiate larger and smaller events. A time window is 5.12 s starting from twice the S wave travel time (Fig. 1b). S wave velocity is assumed as 3300 m/s in this region (e.g., Huang et al. 2017). We use data recorded by more than six stations with a signal-to-noise ratio greater than two within a 0.5 to 30 Hz frequency range. Analysis used as many stations as possible. A total of 20 events forms the cluster advanced to further analysis.

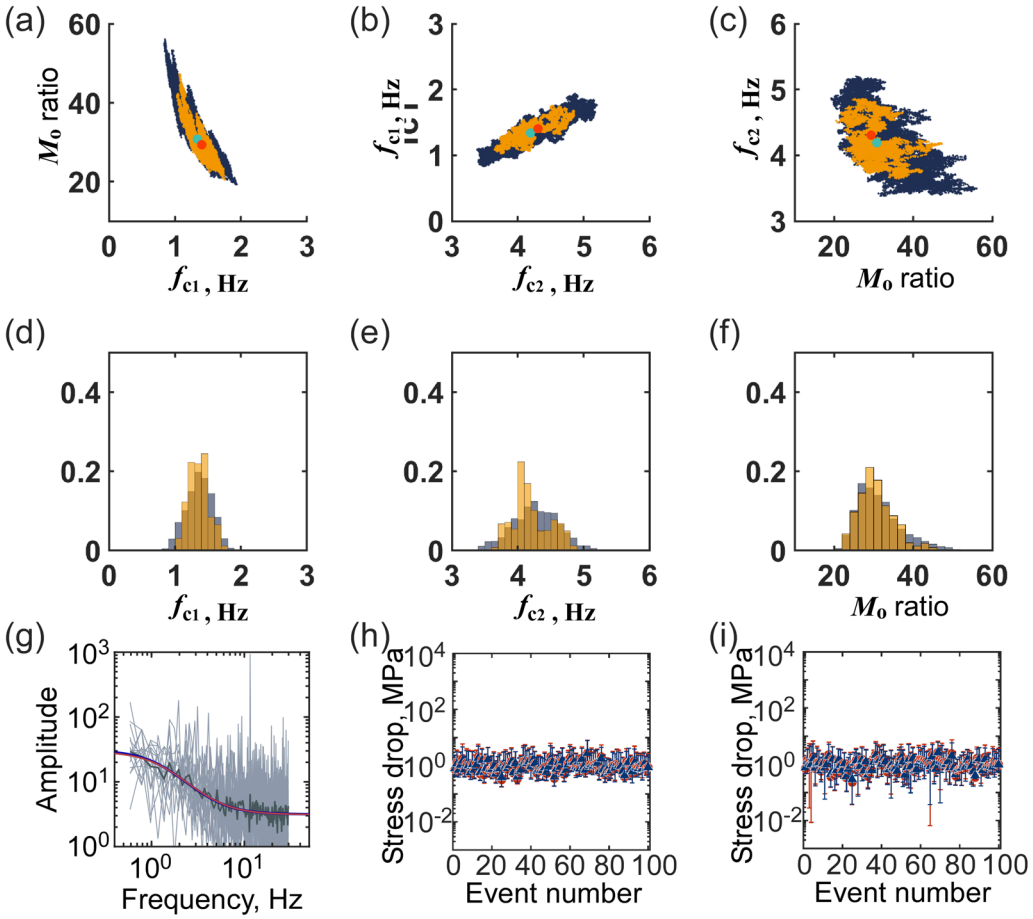

Fig. 2 Source parameters estimated from synthetic data. This calculation is performed for the 8th events in Table 1. **a** Sampling distribution projected onto a 2D plane. Relationship between moment ratio and f_{c1}, **b** f_{c1} and f_{c2}, and **c** moment ratio and f_{c2}. The dark blue areas indicate results assuming an *F*-distribution, and the yellow areas indicate results assuming a normal distribution. Cyan dot and orange circles indicate the highest likelihood estimates for *F*- and normal distribution approaches, respectively. **d** Histogram of the sampling in f_{c1}, **e** f_{c2}, and **f** moment ratio. **g** Synthetic spectral ratios. Gray, black, red curves, respectively, indicate simulated spectral ratio for each seismic station, an average of all spectral ratios, and the theoretical spectral ratio estimated from the best value. **h** Estimated stress drops for 100 trials assuming an *F*-distribution. Red circles indicate the results obtained from large earthquakes, and blue triangles indicate results from small earthquakes. The thin bars indicate a 95% confidence interval obtained from the variation of the accepted sampling. **i** Estimated stress drops for 100 trials assuming a normal distribution. Red circles indicate the results obtained from large earthquakes, and blue triangles indicate results from small earthquakes.

Table 2 (a) Estimated parameters for the first ten events in the synthetic data assuming a F-distribution. Rows list (from left to right) event number, estimated moment ratio, estimated corner frequency of the large earthquake (Hz), the estimated corner frequency of the small earthquake (Hz), stress drop estimated for a large earthquake (MPa), and the stress drop estimated for a small earthquake event (MPa). Thin characters indicates the selected event presented in Fig. 2. (b) Estimated parameters for synthetic data assuming a normal distribution

Event num	Mo ratio	fc1	fc2	Stress drop1	Stress drop2
1	**35.7**	**1.2**	**4.1**	**0.7**	**0.8**
2	**26.8**	**1.4**	**4.2**	**1.3**	**1.2**
3	**33.0**	**1.2**	**3.8**	**0.7**	**0.7**
4	**32.0**	**1.4**	**4.3**	**1.1**	**1.1**
5	**24.2**	**1.6**	**4.4**	**1.7**	**1.5**
6	**36.3**	**1.2**	**4.0**	**0.7**	**0.8**
7	**28.7**	**1.4**	**4.3**	**1.2**	**1.1**
8	30.4	1.3	4.2	1.0	1.0
9	**38.4**	**1.1**	**3.7**	**0.5**	**0.6**
10	**29.6**	**1.4**	**4.3**	**1.1**	**1.1**
(b)					
Event num	**Mo ratio**	**fc1**	**fc2**	**Stress drop1**	**Stress drop2**
1	**34.8**	**1.2**	**4.0**	**0.7**	**0.8**
2	**25.2**	**1.5**	**4.2**	**1.4**	**1.3**
3	**28.2**	**1.4**	**4.2**	**1.2**	**1.1**
4	**33.4**	**1.3**	**4.3**	**1.0**	**1.0**
5	**23.5**	**1.6**	**4.4**	**1.9**	**1.6**
6	**35.7**	**1.2**	**3.9**	**0.7**	**0.7**
7	**28.6**	**1.4**	**4.1**	**1.2**	**1.1**
8	29.3	1.4	4.3	1.2	1.2
9	**38.0**	**1.1**	**3.8**	**0.6**	**0.6**
10	**34.8**	**1.2**	**4.0**	**0.7**	**0.8**

Rows list (from left to right) event number, estimated moment ratio, estimated corner frequency of the large earthquake (Hz), the estimated corner frequency of the small earthquake (Hz), stress drop estimated for a large earthquake (MPa), and the stress drop estimated for a small earthquake event (MPa). Bold indicates the selected event presented in Fig. 2

Results

Initial analysis address synthetic spectral ratios. Figure 2a–g shows an example of this calculation using event number 8, as listed in Table 2. The best-fitting spectral ratios obtained by MCMC calculations are then compared with results derived from probability density functions assuming *F*- and normal distributions. As shown in Fig. 2g, fitted curves obtained from both types of distributions show good agreement with the synthetic records. The sample distribution rendered in three-dimensional (3D) space exhibits a spheroid shape with maximum values at the center indicating the trade-offs between parameters. Histograms of the sampling distribution exhibit the posterior probability distribution. The unimodal distribution of the histogram on the *F*-distribution in Fig. 2e indicates the uniform posterior probability distribution, which is better than the multimodal sampling distribution of the histogram for the normal distribution. A multimodal sampling distribution gives the calculation results including multiple possible results making it difficult to interpret.

Additional file 1: Fig. S1 shows all estimates of the three seismic parameters, seismic moment, f_{c1}, and f_{c2}, with synthetic data. (The subscripts 1 and 2 indicate the larger and smaller earthquake, respectively.) The *F*-distribution input give source parameter means of 32.60 for moment ratio, 1.30 Hz for f_{c1}, and 4.12 Hz for f_{c2}. Standard deviations associated with these parameters are 5.8, 0.19, and 0.33, respectively. The normal distribution gave source parameter means of 32.56 for moment ratio, 1.31 Hz for f_{c1}, and 4.13 Hz for f_{c2}. Standard deviations associated with these values are 6.8, 0.21, and 0.35, respectively. The mean of the estimated parameters show good agreement with input parameters (moment ratio of 31.6, $f_{c1} = 1.3$ Hz, and $f_{c2} = 4.1$ Hz) for both distributions. While corner frequencies show small variation, the seismic moments exhibit relatively larger variance. The variation of estimates associated with the normal distribution also exceeds

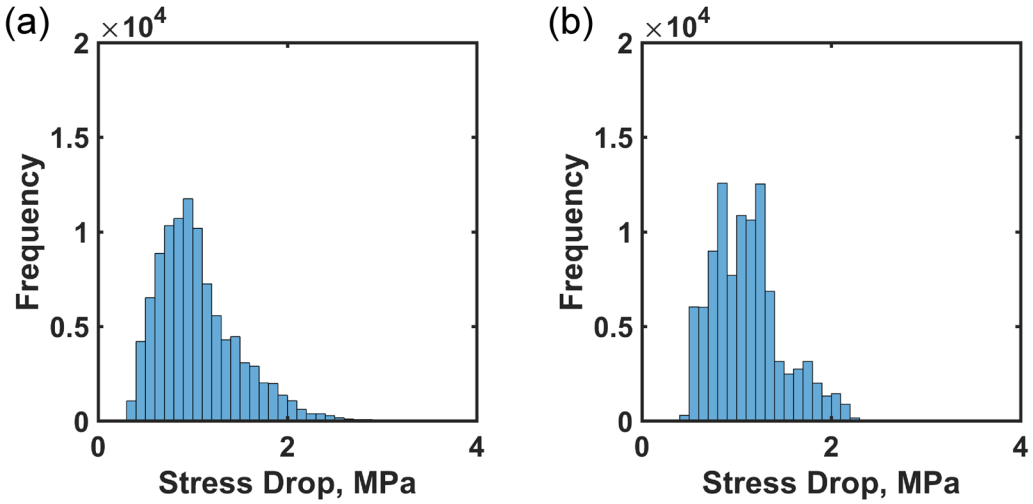

Fig. 3 Histogram of stress drop estimates of a large earthquake with synthetic data **a** assuming an *F*-distribution and **b** normal distribution

that associated with the *F*-distribution. The estimated source parameters, M_o and f_c, are converted into stress drops by using Eq. (1). Since we fix the seismic moment value of the larger event, the smaller seismic moment is indirectly estimated from the moment ratio and the larger moment. Figure 2h, i shows the stress drops estimated from the selected source parameters. The estimates for large earthquakes range from 0.5 MPa to 1.7 MPa for the *F*-distribution and from 0.6 MPa to 1.9 MPa for the normal distribution. The results show good agreement with the given stress drop value of 0.66 MPa. Stress drop estimates for small earthquakes exhibit similar variances as for the larger earthquakes. Comparison of stress drop estimates obtained with the *F*- and normal distributions show no significant differences in their values. The size of the error bars, which reflect the extent of the sampling distribution, is slightly larger for the normal distribution results. Figure 3 shows histograms for stress drops estimated using the *F*- and normal distribution. These indicate posterior distribution for the stress drop. Figure 3b shows a multimodality of the stress drop with normal distribution that may include larger uncertainties on the stress drop while Fig. 3a shows a unimodal distribution. These characteristics of the stress drop distribution reflect the sampling distributions in Fig. 2d–f.

Table 3 lists observed data parameters. Figure 4g shows an example of a spectral ratio from the cluster. Similar to calculations based on synthetic spectral ratios, best-fit curves obtained with *F*- and normal distributions show good agreement with observed spectral ratios. However, the sampling distributions produced by the two different probability density functions exhibits different shapes (Fig. 4a–f). The best sampling point (the highest likelihood value) occur in the center of the sample for the *F*-distribution and at the edge of the sample for the normal distribution. The shape of the sampling distribution derived from a normal distribution is also coarser than that derived from the *F*-distribution. Histograms show multimodal distribution for the sampling based on the normal distribution while histograms for the *F*-distribution show a unimodal shape. All best-fit curves in a cluster show good agreement with theoretical spectral ratios for both types of input probability density function, but their sampling distributions are different.

Figure 4h, i shows stress drops estimates for a 95% confidence interval obtained from variation in sampling. The majority of the stress drops range from 0 to 1 MPa in both probability density functions. Because all spectral ratios in the cluster refer to the common large event, stress drops for large events in the cluster should have similar values. Red circles in Fig. 4h, i indicating stress drops estimated for large events show variation among event pairs. Some event pairs show unusually large stress drops (>100 MPa) relative to other event pairs. Stress drop estimates based on a normal distribution input exhibit more significant variation and errors than those based on *F*-distributions.

Discussion

Probability density functions in a Bayesian framework

When used as input functions for the methods described above, an *F*-distribution gives different results from a normal distribution. Variation in the sampling distribution relates to uncertainties estimated from the 95% confidence interval. Confidence intervals in Fig. 4h, i indicate a large estimation error in results based on normal distribution assumptions. The distorted and coarse shape of the

Table 3 (a) Estimated parameters for observational data assuming a *F*-distribution. From left to right, rows list event number, estimated moment ratio, corner frequency (Hz), stress drop estimated for a large earthquake (MPa), and the stress drop of a small earthquake (MPa). Events with thin characters mean that the event is not selected. (b) The estimated parameters for observational data assuming a normal distribution

Event num	Moment ratio	Fc1	Fc2	Stress drop1	Stress drop2
1	325.3	0.3	1.4	0.02	0.003
2	24.4	8.3	8.6	241.3	11.1
3	1.0	3.5	3.4	18.4	16.4
4	**27.7**	**1.2**	**1.9**	**0.7**	**0.1**
5	**28.4**	**1.1**	**2.0**	**0.6**	**0.1**
6	**70.5**	**0.9**	**2.1**	**0.3**	**0.1**
7	**44.1**	**1.0**	**2.4**	**0.5**	**0.1**
8	**21.7**	**1.0**	**1.5**	**0.4**	**0.1**
9	2.8	3.6	3.4	19.7	5.9
10	**29.8**	**0.7**	**1.8**	**0.1**	**0.1**
11	**31.4**	**0.7**	**1.8**	**0.1**	**0.1**
12	24.2	1.1	2.1	0.6	0.2
13	**43.4**	**0.8**	**1.6**	**0.3**	**0.04**
14	**74.7**	**0.9**	**2.1**	**0.3**	**0.1**
15	20.9	8.8	14.0	290.7	56.0
16	**21.0**	**0.8**	**1.9**	**0.2**	**0.1**
17	21.2	13.4	18.6	1030.2	129.8
18	**14.4**	**0.9**	**1.9**	**0.3**	**0.2**
19	42.6	6.2	8.0	101.3	5.2
20	**78.6**	**1.6**	**3.2**	**1.8**	**0.2**

(b)

	Moment ratio	fc1	fc2	Stress drop1	Stress drop2
1	**28.8**	**3.7**	**4.5**	**22.0**	**1.3**
2	**24.6**	**5.7**	**5.8**	**78.4**	**3.5**
3	**0.9**	**4.3**	**3.9**	**33.0**	**27.3**
4	**15.6**	**3.7**	**4.3**	**21.0**	**2.2**
5	**25.9**	**1.1**	**1.8**	**0.5**	**0.1**
6	**53.1**	**0.9**	**2.0**	**0.3**	**0.1**
7	**43.5**	**0.9**	**2.1**	**0.4**	**0.1**
8	**12.4**	**2.6**	**3.2**	**7.7**	**1.1**
9	**2.4**	**4.9**	**4.1**	**49.2**	**12.4**
10	**23.1**	**0.7**	**1.6**	**0.1**	**0.1**
11	**26.4**	**0.6**	**1.5**	**0.1**	**0.1**
12	**32.8**	**0.9**	**2.0**	**0.3**	**0.1**
13	**16.7**	**5.1**	**6.4**	**56.1**	**6.6**
14	**82.4**	**0.8**	**1.9**	**0.2**	**0.03**
15	**50.8**	**1.1**	**2.3**	**0.5**	**0.1**
16	**14.8**	**0.9**	**1.8**	**0.3**	**0.2**
17	**20.3**	**5.6**	**6.8**	**76.6**	**6.6**
18	**11.0**	**1.0**	**1.9**	**0.4**	**0.3**
19	**74.9**	**2.0**	**3.6**	**3.3**	**0.3**
20	**92.0**	**1.1**	**2.4**	**0.6**	**0.1**

From left to right, rows list event number, estimated moment ratio, corner frequency (Hz), stress drop estimated for a large earthquake (MPa), and the stress drop of a small earthquake (MPa). Events with bold mean that the event is not selected

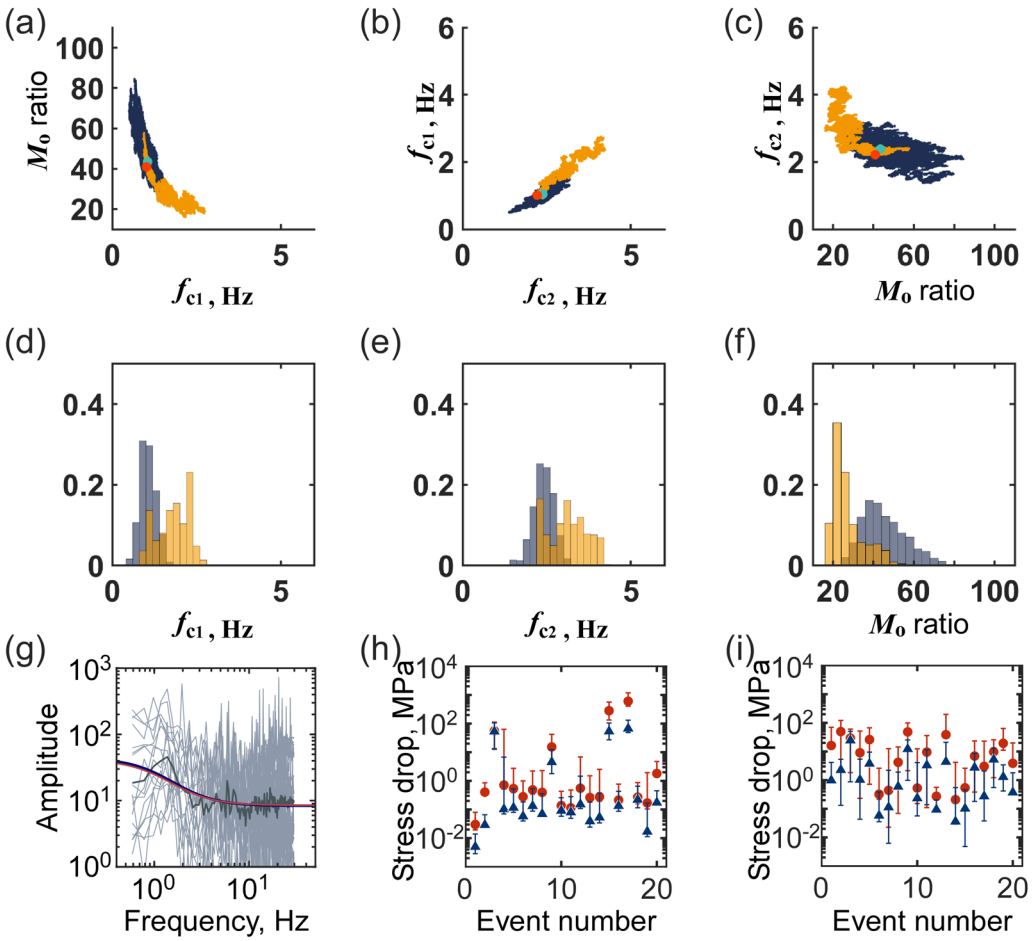

Fig. 4 Seismic parameters estimated from observational data subjected to 200,000 iterations of MCMC analysis. **a** Sampling distribution projected onto a 2D plane. Relationship between moment ratio and f_{c1}, **b** f_{c1} and f_{c2}, and **c** moment ratio and f_{c2}. Dark blue areas indicate results assuming an *F*-distribution, and yellow areas indicate results assuming a normal distribution. Cyan and orange dots indicate the best point of the calculation, respectively. **d** Histogram of the sampling in f_{c1}, **e** f_{c2}, and **f** moment ratio. **g** Spectral ratios of the 7th event in Table 1. Gray, black, and red curves, respectively, indicate spectral ratio for each seismic station, average of all spectral ratios, and the theoretical spectral ratio based on the maximum likelihood value. **h** Estimated stress drops for 20 events from a cluster assuming an *F*-distribution. Red circles indicate the results obtained from large earthquakes, and blue triangles indicate results obtained from small earthquakes. The thin bars indicate 95% confidence interval obtained from the variation of the accepted sampling. **i** Estimated stress drops for 20 events from a cluster assuming a normal distribution. Red circles indicate results obtained from large earthquakes, and blue triangles indicate results obtained from small earthquakes

sampling based on normal distribution assumptions may arises from an insufficient number of iterations generating unstable results. We therefore increase the number of iterations from 200,000 to 400,000 and run the MCMC steps again (Fig. 5). The characteristics of the sampling distribution, stress drop estimates, and errors for the 400,000 iteration runs indicate similar tendencies to the results obtained from the 200,000 iterations runs. Thus, calculations based on *F*-distribution assumptions gave denser sampling distribution relative to those based on normal distribution assumptions. Several best parameters appear within tail areas of the sampling distribution for the calculation based on normal distribution assumptions.

F-distribution assumptions are appropriate for the spectral ratio data and appear to perform robustly when the shape of spectra is disturbed from its ideal form. When we use an *F*-distribution to interpret the observed spectral ratio, the log-likelihood function is approximated by $-|x-m|$ where x is the logarithm of the observed spectral ratio and m is the logarithm of the theoretical spectral ratio. For a normal distribution, the log-likelihood function is proportional to $-(x-m)^2$ and thus becomes more sensitive to outliers. Along with characteristics of a sampling distribution and the error of the estimated stress drops, these factors make *F*-distribution

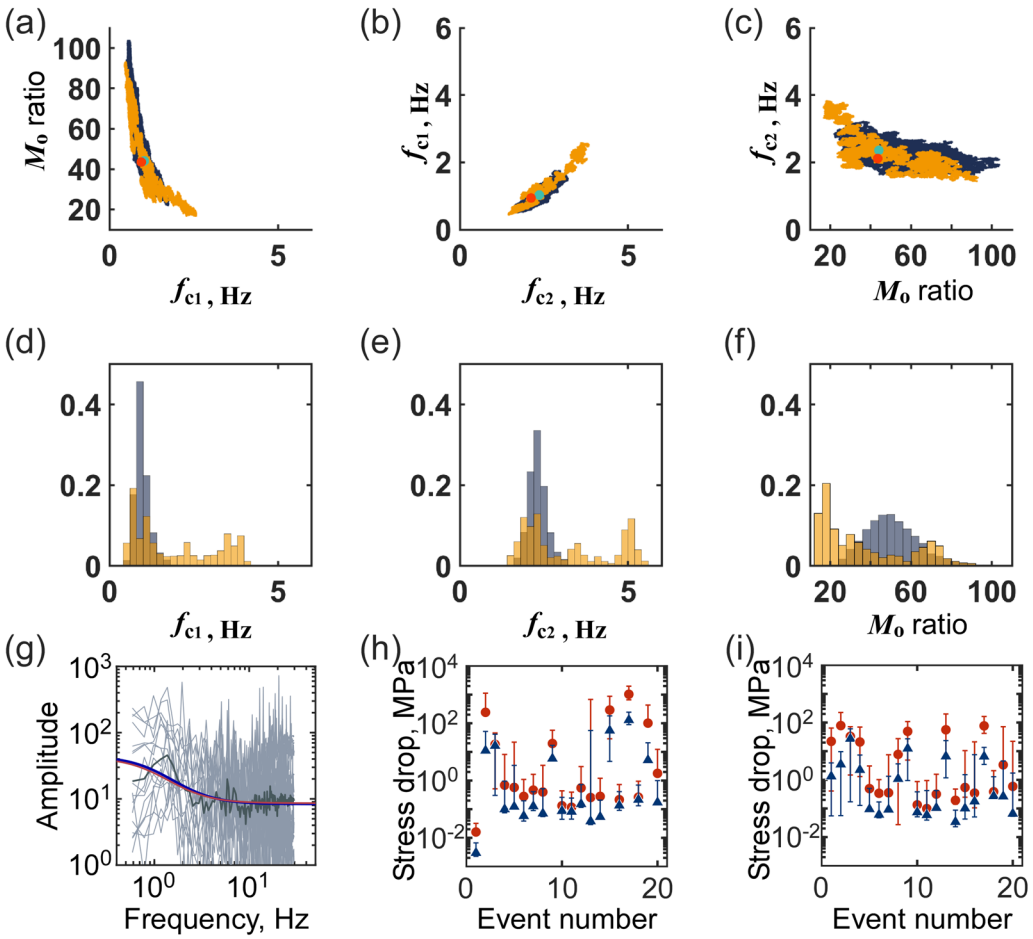

Fig. 5 Source parameters calculated from observational data subjected to 400,000 iterations of MCMC analysis. **a** Sampling distribution projected onto a 2D plane. Relationships between moment ratio and f_{c1}, **b** f_{c1} and f_{c2}, and **c** moment ratio and f_{c2}. The dark blue areas indicate results assuming an *F*-distribution, and the yellow areas indicate results assuming a normal distribution. Cyan and orange circle indicate the highest likelihood values from the *F*- and normal distribution calculations, respectively. **d** Histogram of the sampling in f_{c1}, **e** f_{c2}, and **f** moment ratio. **g** Spectral ratios of the 7th event in Table 1. Gray, black, and red curves, respectively, indicate spectral ratios for each seismic station, an average of all spectral ratios, and the theoretical spectral ratio according to the highest likelihood values. **h** Estimated stress drops for 20 events in a cluster assuming an *F*-distribution. Red circles indicate results obtained from large earthquakes, and blue triangles indicate results obtained from the smaller earthquake. The thin bars indicate a 95% confidence interval obtained from the variation of the accepted sampling. **i** Estimated stress drops assuming a normal distribution. Red circles indicate results obtained from large earthquakes, and blue triangles indicate results obtained from smaller earthquakes.

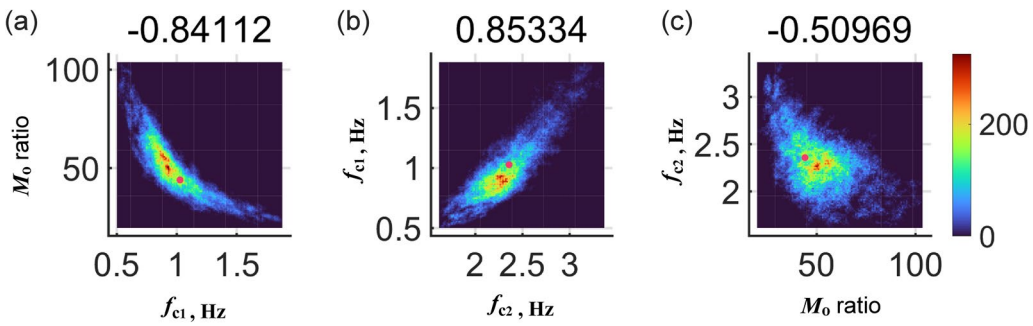

Fig. 6. 2D histogram based on sampling distribution. Color scales indicate the density of the sample. Pink circles indicate the highest likelihood values from the *F*-distribution. The value displayed on each panel indicates the correlation coefficient

assumptions more suitable than normal distribution assumptions for the methods under consideration.

Calculations with observational data assuming the two different types of probability density functions gave different sampling distributions and histograms after 400,000 iterations, whereas results from synthetic data show only small differences. Differences in results between observational and synthetic data may arise from several sources. First, synthetic data in this study assume that events occurred at identical locations, whereas observed events occurred at similar but slightly different locations. Secondly, observed waves, including the coda part of the waveform, record anisotropic radiation patterns and directivity effects. Thirdly, variations in the amplitude of the spectral ratio for each station (gray curve in Figs. 2g and 5g) differ for synthetic and observed data. Since we use the raw spectral record of all stations instead of smoothed, stacked data, the amplitude and shape of the original data will contribute to variation in the results.

Figure 6 shows the two-dimensional (2D) histogram indicating a marginal distribution (e.g., Supino et al. 2019). While Fig. 6 exhibits dense sampling in the central part of the distribution, multiple peaks appear in the high density sampling. It is interesting to note that the position of the peak sampling density is not the same as the position of the highest likelihood. This arises from differences between the sampling density in different dimensions as a dense sampling region in 3D space may not transpose when integrated into 2D space.

Trade-offs among parameters

Sampling distributions obtained from all 100 synthetic spectral ratios and most of the observed spectral ratios show similar relationships among parameters (Fig. 2 a–c). The sampling distributions for both f_{c1} and M_o, and f_{c2} and M_o show negative correlations, while f_{c1} and f_{c2} show a positive correlation. These relations indicate the trade-offs among parameters. The term f_{c1} exhibits a lesser degree of variation in its distributional range relative to that of f_{c2}. Similar to relations reported by previous studies, the spectrum covering the higher frequency range is less stable than that covering the lower frequency range. This high frequency disturbance arises from high-frequency radiation of smaller magnitude events, observation noise, and tremor-like noise. This contributes to larger estimation errors for corner frequency parameter f_{c2} relative to that for f_{c1}. The seismic moment also shows a relatively wide distribution.

Trade-offs between source parameters also influence the stress drop. Figure 7a shows the sampling distribution for the stress drop converted from a sampling of source parameters. The sampling distributions for the stress drop derived from synthetic data show a strong positive relationship between large and small earthquakes. Observational data also show a similarly strong positive correlation between samples of two stress drops (Fig. 7b). In the case of observational data, the stress drop of smaller earthquakes shows smaller values than that of larger earthquakes. In this study, we set M_{01} as a known value and indirectly estimate M_{02} from M_R. When we calculate

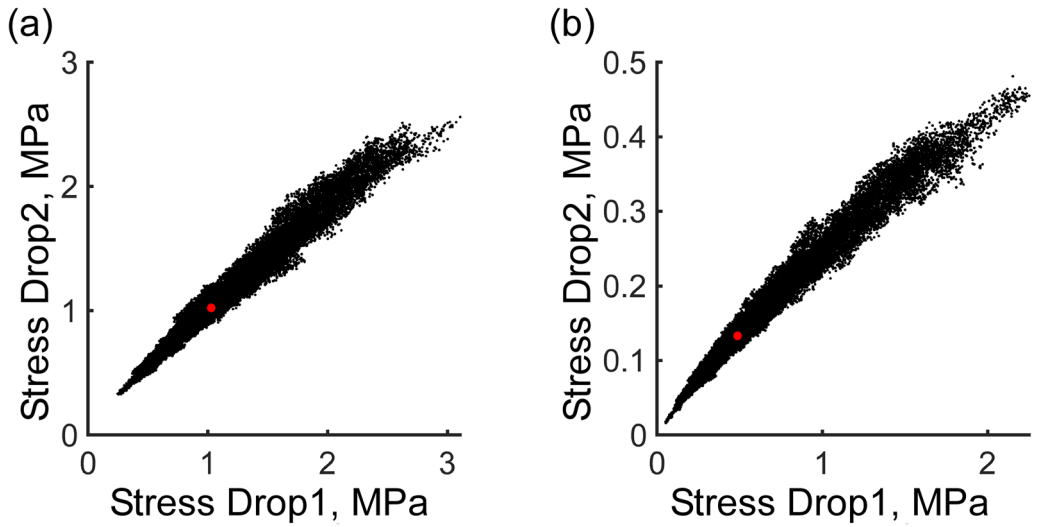

Fig. 7 Sampling distribution of stress drop with **a** synthetic data and **b** observational data (7th event in Table 1). The horizontal axis indicates stress drop estimated from large earthquakes, and the vertical axis indicates stress drop estimated from small earthquakes

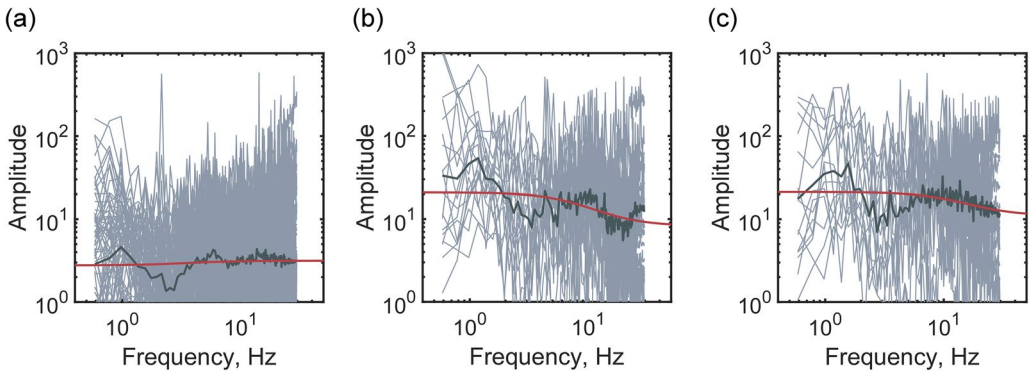

Fig. 8 Example of spectral ratios. **a** Spectral ratio removed according to selection criteria. **b**, **c** Spectral ratios show unusually large stress drop

the stress drop from the spectral ratio, the stress drop of the larger event, $\Delta\sigma_1$, is proportional to $M_{01}f_{c1}^3$ and the stress drop of the smaller event, $\Delta\sigma_2$, is proportional to $(M_{01}/M_R)f_{c2}^3$. This study uses only one large event, thus M_{01} is a constant. The pronounced trends of M_R's inverse proportionality to f_{c1}, and f_{c1}'s proportionality to f_{c2} (Fig. 2a) indicate that $\Delta\sigma_2$'s estimation quality exhibits larger estimation bias than that of $\Delta\sigma_1$ and depends on both M_R and f_{c1}.

Stress drop estimates

Some seismic events in our study exhibit unusually large stress drops even after a sufficient number of iterations. Because we use a single large event to calculate the spectral ratio with different small events, the stress drop estimates for larger earthquakes should give similar values for event pairs. The raw spectral ratios with unusually large stress drop values, however, do not exhibit theoretical stair-like spectral ratios. In spite of the care taken, data selection sometimes included disordered waveforms. Among the irregular shapes observed, one consists of an almost flat plateau across the entire frequency range (Fig. 8a), while another of many ups and downs (Fig. 8b, c). Previous research with conventional grid search analysis has also reported similar problems wherein irregularly shaped spectral ratios influence the quality of stress drop estimates (Prieto 2007; Uchide and Imanishi 2016; Yoshimitsu et al. 2019).

As shown in Additional file 1: Fig S2, distorted sampling distributions appear in association with irregular stress drops. To remove the results with irregularly shaped spectral ratios and irregular stress drops, we evaluate the shape of the sampling distribution. Calculations assuming an *F*-distribution give a relatively tight, unimodal histogram, whereas irregular stress drop events give a more sparsely sampled, multimodal histogram. As described in the trade-off section, sampling distributions for typical stress drop events exhibit a negative

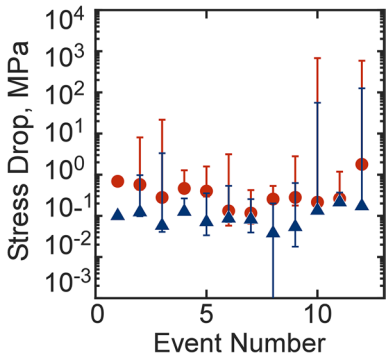

Fig. 9 Stress drops within an earthquake cluster after event selection. Red circles indicate the results obtained from large earthquakes, and blue triangles indicate results obtained from smaller earthquakes. The original figure before the event selection is Fig. 5h

correlation between f_{c1} and seismic moment, positive correlation between f_{c1} and f_{c2}, and negative correlation between seismic moment and f_{c2} for synthetic spectral ratios. Sampling distributions with contrasting correlation patterns or distorted shapes, give estimated stress drops with irregular values. Thus, the correlation patterns in the sampling distribution can help distinguish irregular stress drop events.

We assume that correlations in results derived from synthetic data represent ideal trends and examine the agreement of the positive or negative trend in sampling distribution among each parameter pair in the observed data. Following Supino et al. (2019), we calculate correlation coefficients of the sampling with two parameters shown in Fig. 6. We select events that adhered to the correlation trend described above and which gave high correlation (>0.5) coefficients. Figure 5a–c shows observational data filtered according to these criteria gives sampling trends similar to those derived from synthetic results. Figure 9 shows cluster stress drop estimates after using this selection process. Exclusion of irregular

sampling distribution yields stress drop estimates for large events that, for most cases, vary almost within one order. The relatively small size of this parameter demonstrates that these steps can consistently achieve precise results.

Comparison of stress drop estimates with the *F*-distribution in Fig. 5h and 9 demonstrates the effects of this selection strategy. Very high or low estimates disappeared after selection. We conclude that probability density function selection influences both calculation results and posterior evaluation of event quality. As noted above, irregular stress drops in Fig. 5h give irregularly shaped spectral ratios. Tables 1 and 3 show the selected/unselected events list. These document the absence of temporal or spatial characteristics for selected events. Given the use of events occurring in similar locations there may relate to differences in the individual source processes instead of the path effect.

Concluding remarks

This study uses an *F*-distribution as a probability density function for MCMC calculation of seismic source parameters. The *F*-distribution is well-suited for data that take the form of ratios. The study evaluates sampling distributions and obtains source parameters to find that the *F*-distribution generates more accurate results than a normal distribution. Using the sampling distribution obtained from MCMC iterations, we evaluate trade-offs between estimated source parameters. Most event pairs in the cluster show similar sampling distribution trends if the form of their spectral ratio resembles that estimated from theoretical inputs. The correlation coefficient of the sampling pattern permits identification and exclusion of results derived from the irregularly shaped spectral ratios. Estimate quality of source parameters improves with a number of iterations. Calculations using a large number of iterations and event selection based on the sampling trend give stress drop estimates with a relatively small degree of variation in a cluster.

Supplementary Information

The online version contains supplementary material available at https://doi.org/10.1186/s40623-023-01770-2.

Additional file 1: **Figure S1**. Estimates of seismic parameters calculate from synthetic spectral ratios, assuming (a) an *F*-distribution and (b) a normal distribution. Top panels indicate the result of seismic moment, middle panels indicate the result of f_{c1}, and the bottom panels indicate the result of f_{c2}. **Figure S2**. Sampling distribution of project onto a 2D plane with irregular spectral shape. (a), (b), and (c) represent the sampling distributions obtained from the event in Fig. 8(a). (d), (e), and (f) are obtained from the event in Fig. 8(b). (g), (h), and (i) are obtained from the event in Fig. 8(c). (a), (d), and (g) indicate the relationships between moment ratio and f_{c1}. (b), (e), and (h) indicate the relationships between f_{c1} and f_{c2}. (c), (f), and (i) indicate the relationship between moment ratio and f_{c2}. **Figure S3**. Stress drops within an earthquake cluster after event selection. Red circles indicate the results obtained from large earthquakes, and blue triangles indicate results obtained from smaller earthquakes. Dark color obtained from the source model proposed by Brune (1970) and light color obtained from the source model proposed by Madariaga (1976).

Acknowledgements
We thank JST and JSPS for their support of this study.

Author contributions
NY performed analysis and wrote the manuscript. NY, TM and TS improved analytical methods and interpreted the results. All authors read and approved the final manuscript.

Funding
This work is supported by JST CREST Grant JPMJCR1763 and ERI JURP 2022-A-02 in Earthquake Research Institute, the University of Tokyo. NY is supported by JSPS KAKENHI, Grant Number 19K14812.

Availability of data and materials
Seismic data used in this study are available through IRIS Data Management Center (http://ds.iris.edu/ds/nodes/dmc/data/types/waveform-data/).

Declarations

Competing interests
The authors declare that they have no competing interests.

Author details
[1]Department of Civil and Earth Resources Engineering, Kyoto University, C1-3, Katsura Campus, Nishikyo-Ku, Kyoto 615-8540, Japan. [2]Graduate School of Science and Technology, Hirosaki University, 3 Bunkyo-Cho, Hirosaki-Shi, Aomori 036-8561, Japan. [3]Graduate School of Information Science and Technology, The University of Tokyo, 7-3-1 Hongo, Bunkyo-Ku, Tokyo 113-8656, Japan.

Received: 6 May 2022 Accepted: 14 January 2023
Published online: 08 March 2023

References

Abercrombie RE (1995) Earthquake source scaling relationships from − 1 to 5 ML using seismograms recorded at 2.5-km depth. J Geophys Res Solid Earth 100(B12):24015–24036. https://doi.org/10.1029/95JB02397

Abercrombie RE, Trugman DT, Shearer PM, Chen X, Zhang J, Pennington CN, Hardebeck JL, Goebel THW, Ruhl CJ (2021) Does earthquake stress drop increase with depth in the crust? J Geophys Res Solid Earth. https://doi.org/10.1029/2021JB022314

Aki K, Richards PG (1980) Quantitative seismology: theory and methods. W H Freeman and Company, San Francisco

Allmann BP, Shearer PM (2009) Global variations of stress drop for moderate to large earthquakes. J Geophys Res Solid Earth 114:B01310. https://doi.org/10.1029/2008JB005821

Baltay AS, Hanks TC, Abrahamson NA (2019) Earthquake stress drop and Arias intensity. J Geophys Res Solid Earth 124:3838–3852. https://doi.org/10.1029/2018JB016753

Berg EM, Lin F-C, Allam A, Schulte-Pelkum V, Ward KM, Shen W (2020) Shear velocity model of Alaska via joint inversion of Rayleigh wave ellipticity, phase velocities, and receiver functions across the Alaska Array. J Geophys Res Solid Earth. https://doi.org/10.1029/2019JB018582

Brune JN (1970) Tectonic stress and the spectra of seismic shear waves from earthquakes. J Geophys Res 75:4997–5009. https://doi.org/10.1029/JB075i026p04997

Brune JN (1971) Tectonic stress and seismic shear waves from earthquakes, correction. J Geophys Res 76:5002. https://doi.org/10.1029/JB076i020p05002

Casella G, Berger RL (2002) Statistical Inference, 2nd edn. CA, Duxbury Press, Pacific Grove
Chu S, Beroza GC, Ellsworth WL (2019) Source parameter variability of intermediate-depth earthquakes in Japanese subduction zones. J Geophys Res Solid Earth 124:8704–8725. https://doi.org/10.1029/2019JB017592
Cotton F, Archuleta R, Mathieu C (2013) What is sigma of the stress drop? Seismol Res Lett 84:42–48. https://doi.org/10.1785/0220120087
Eshelby JD (1957) The determination of the elastic field of an ellipsoidal inclusion, and related problems. Proc R Soc Lond A241:376–396. https://doi.org/10.1098/rspa.1957.0133
Godano M, Bernard P, Dublanchet P (2015) Bayesian inversion of seismic spectral ratio for source scaling: application to a persistent multiplet in the western Corinth rift. J Geophys Res Solid Earth 120:7683–7712. https://doi.org/10.1002/2015JB012217
Goebel THW, Hauksson E, Shearer PM, Ampuero JP (2015) Stress-drop heterogeneity within tectonically complex regions: a case study of San Gorgonio Pass, Southern California. Geophys J Int 202:514–528. https://doi.org/10.1093/gji/ggv160
Hanks TC (1977) Earthquake stress drops, ambient tectonic stresses and stresses that drive plate motions. Pure Appl Geophys 115:441–458. https://doi.org/10.1007/BF01637120
Hough SE (1997) Empirical green's function analysis: taking the next step. J Geophys Res Solid Earth 102(B3):5369–5384. https://doi.org/10.1029/96JB03488
Huang Y, Ellsworth WL, Beroza GC (2017) Stress drops of induced and tectonic earthquakes in the central United States are indistinguishable. Sci Adv 3:1700772. https://doi.org/10.1126/sciadv.1700772
Imanishi K, Ellsworth WL (2006) Source scaling relationships of microearthquakes at Parkfield, CA, determined using the SAFOD pilot hole seismic array. In: Abercrombie R, McGarr A, Di Toro G, Kanamori H (eds) earthquakes: radiated energy and the physics of faulting. American Geophysical Union, Washington DC
Kwiatek G, Plenkers K, Dresen G, JAGUARS Research Group (2011) Source parameters of picoseismicity recorded at Mponeng deep gold mine, South Africa: implications for scaling relations. Bull Seismol Soc Am 101:2592–2608. https://doi.org/10.1785/0120110094
Lomax A, Virieux J, Volant P, Berge-Thierry C (2000) Probabilistic Earthquake Location in 3D and Layered Models. In: Thurber CH, Rabinowitz N (eds) Advances in seismic event location modern approaches in geophysics. Springer, Dordrecht
Madariaga R (1976) Dynamics of an expanding circular fault. Bull Seismol Soc Am 66(3):639–666
Mayeda K, Malagnini L, Walter WR (2007) A new spectral ratio method using narrow band coda envelopes: evidence for non-self-similarity in the Hector Mine sequence. Geophys Res Lett 34:L11303. https://doi.org/10.1029/2007GL030041
Metropolis N, Rosenbluth AW, Rosenbluth MN, Teller AH, Teller E (1953) Equation of state calculations by fast computing machines. J Chem Phys 21:1087–1092. https://doi.org/10.1063/1.1699114
Oth A (2013) On the characteristics of earthquake stress release variations in Japan. Earth Planet Sci Lett 377–378:132–141. https://doi.org/10.1016/j.epsl.2013.06.037
Prieto GA, Thomson DJ, Vernon FL, Shearer PM, Parker RL (2007) Confidence intervals for earthquake source parameters. Geophys J Int 168:1227–1234. https://doi.org/10.1111/j.1365-246X.2006.03257.x
Roy C, Romanowicz BA (2017) On the implications of a priori constraints in transdimensional Bayesian inversion for continental lithospheric layering. J Geophys Res Solid Earth 122:10118–10131. https://doi.org/10.1002/2017JB014968
Sambridge M, Mosegaard K (2002) Monte Carlo methods in geophysical inverse problems. Rev Geophys 40(3):1009. https://doi.org/10.1029/2000RG000089
Supino M, Festa G, Zollo A (2019) A probabilistic method for the estimation of earthquake source parameters from spectral inversion: application to the 2016–2017 Central Italy seismic sequence. Geophys J Int 218(2):988–1007. https://doi.org/10.1093/gji/ggz206
Uchide T, Imanishi K (2016) Small earthquakes deviate from the omega-square model as revealed by multiple spectral ratio analysis. Bull Seismol Soc Am 106:1357–1363. https://doi.org/10.1785/0120150322
Wu Q, Chapman M (2017) Stress-drop estimates and source scaling of the 2011 Mineral, Virginia, mainshock and aftershocks. Bull Seismol Soc Am 107:2703–2720. https://doi.org/10.1785/0120170098
Yamada T, Mori JJ, Ide S, Abercrombiem RE, Kawakata H, Nakatani M, Iio Y, Ogasawara H (2007) Stress drops and radiated seismic energies of microearthquakes in a South African gold mine. J Geophys Res Solid Earth 112:B03305. https://doi.org/10.1029/2006JB004553
Yoon CE, Yoshimitsu N, Ellsworth WL, Beroza GC (2019) Foreshocks and mainshock nucleation of the 1999 Mw 7.1 Hector Mine, California, earthquake. J Geophys Res Solid Earth 124:1569–1582. https://doi.org/10.1029/2018JB016383
Yoshimitsu N, Ellsworth WL, Beroza GC (2019) Robust stress drop estimates of potentially induced earthquakes in Oklahoma: evaluation of empirical Green's function. J Geophys Res Solid Earth 124:5854–5866. https://doi.org/10.1029/2019JB017483

Publisher's Note